

SynthRender and IRIS: Open-Source Framework and Dataset for Bidirectional Sim–Real Transfer in Industrial Object Perception

Jose Moises Araya-Martinez^{1,2,3,*}, Thushar Tom^{2,†}, Adrián Sanchis Reig^{2,†}, Pablo Rey Valiente², Jens Lambrecht⁴, and Jörg Krüger¹

Abstract—Object perception is fundamental for tasks such as robotic material handling and quality inspection. However, modern supervised deep-learning perception models require large datasets for robust automation under semi-uncontrolled conditions. The cost of acquiring and annotating such data for proprietary parts is a major barrier for widespread deployment. In this context, we release SynthRender, an open source framework for synthetic image generation with Guided Domain Randomization capabilities. Furthermore, we benchmark recent Reality-to-Simulation techniques for 3D asset creation from 2D images of real parts. Combined with Domain Randomization, these synthetic assets provide low-overhead, transferable data even for parts lacking 3D files. We also introduce IRIS, the Industrial Real-Sim Imagery Set, containing 32 categories with diverse textures, intra-class variation, strong inter-class similarities and about 20,000 labels. Ablations on multiple benchmarks outline guidelines for efficient data generation with SynthRender. Our method surpasses existing approaches, achieving 99.1% mAP@50 on a public robotics dataset, 98.3% mAP@50 on an automotive benchmark, and 95.3% mAP@50 on IRIS.

I. INTRODUCTION

Visual object perception is essential for robust automation of complex tasks in semi-uncontrolled industrial environments. Tasks such as robot-based bin-picking and box handling [1], as well as quality inspection [2], exhibit high automation potential. Recent foundational models enable training-free pose estimation [3] and semantic segmentation [4], but they still require prior object detection to handle unknown objects. Modern detectors, however, rely on supervised, data-intensive learning [5], [6], creating a bottleneck for widespread industrial adoption. This work addresses this challenge via efficient synthetic training. Fig. 1 shows the three main stages of our approach.

First, we generate a graphics database of target and scene 3D assets. If Computer-Aided Design (CAD) files are available, they are directly used; otherwise, we employ 3D Gaussian Splatting (3DGS) [7] and GenAI methods for low-overhead 3D reconstruction from 2D images. Second, Syn-

This work was funded by the German Federal Ministry for Economic Affairs and Climate Action based on a resolution of the German Bundestag, and financed by the European Union. We gratefully acknowledge FATH GmbH, Festo SE & Co. KG, GlobalFastener Inc., and McMaster-Carr Supply Co. for granting permission to include selected 3D models in the IRIS dataset. All copyrights remain with their respective owners.

¹Technical University Berlin, Industrial Automation Technology.

²Mercedes-Benz AG, Future Manufacturing Technologies.

³ARENA2036 e.V., Industrial Metaverse.

⁴Technical University Berlin, Industry Grade Networks and Clouds.

*Corresponding author: araya.martinez@campus.tu-berlin.de.

[†]Equal contribution.

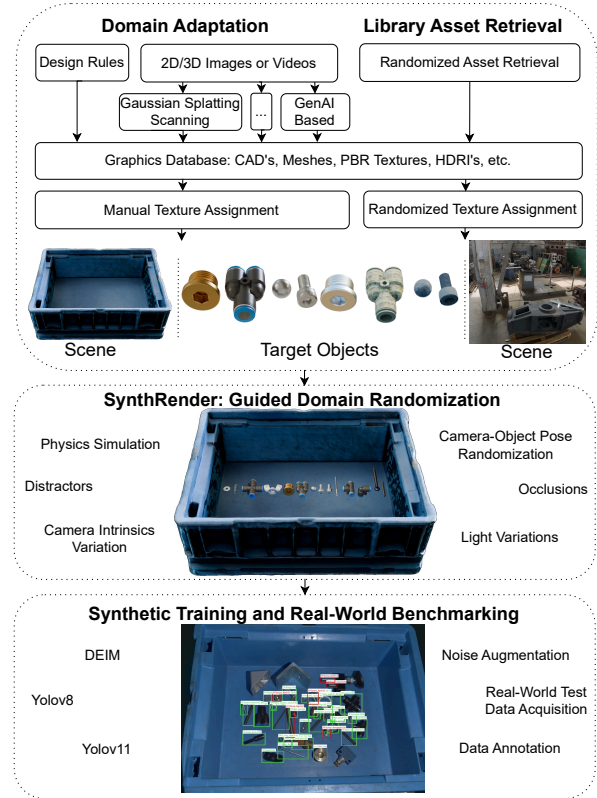


Fig. 1: Architecture for efficient domain adaptation, domain randomization, and bidirectional sim-real gap reduction.

thRender, our BlenderProc-based [8] synthesizer, generates diverse data via Domain Randomization (DR) or Guided DR when target conditions are known. SynthRender includes physics simulation [9] for realistic object placement and three-point lighting with controllable intensity. Finally, IRIS provides real and synthetic imagery with both CAD models and reconstructed assets, enabling systematic evaluation of bidirectional sim-real transfer.

Our contributions are summarized as follows:

a) *Sim-to-real SynthRender Framework*: An open-source framework implementing Guided Domain Randomization (GDR) for industrial perception. Systematic ablations across three benchmarks identify key design principles: physics-based placement, exponential light sampling, RGB lighting, and material randomization. SynthRender surpasses prior pipelines, demonstrating that *how* synthetic variability is constructed matters more than dataset scale or detec-

tor architecture. SynthRender is built on BlenderProc [8], [10] and is available at <https://github.com/Moiso/SynthRender.git>.

b) Automated Domain Adaptation (DA) Methods: We benchmark multiple low-overhead DA strategies to create 3D assets from 2D images, including GenAI for 2D-to-3D generation [11], Gaussian Splatting for mesh generation [7], and texture inference for context-aware synthetic data [12].

c) The Industrial Real-Sim Imagery Set (IRIS): Designed for sim-to-real benchmarking in semi-uncontrolled industrial environments. IRIS contains CADs and reconstructed meshes for 32 objects, 508 high-resolution RGB-D images annotated for object detection. IRIS also includes 8,000 synthetic high-variation images from SynthRender which led to our best results. IRIS is available at <https://huggingface.co/datasets/moiaraya/IRIS>.

d) Ablation Studies: Comprehensive experiments quantify the impact of each component, guiding design decisions that enable state-of-the-art performance on a public robotics dataset [13], [14] and an automotive benchmark [15].

In short, our work investigates how low-overhead DA (3D generation) in combination with programmatic physically-grounded GDR (SynthRender) provide data-efficient sim-to-real transfer in multiple industrial benchmarks. Furthermore, we validate this results on IRIS, a novel bidirectional sim-real dataset. Following standard object detection benchmarks, we report Mean Average Precision (mAP) at a 50% Intersection over Union (IoU) threshold (mAP@50) [16] and COCO-style mAP averaged over IoU thresholds from 50% to 95% in 5% steps (mAP@50–95) [17].

The next section reviews the current state-of-the-art in industrial domain randomization and adaptation. We then describe the 2D-to-3D generation techniques employed in our methodology, followed by our SynthRender framework, and our IRIS dataset. Subsequently, we present and discuss the results of multiple ablation studies. Finally, we draw conclusions and outline directions for future work.

II. RELATED WORKS

This section reviews previous works on data-centric approaches pursuing to alleviate the latent data bottleneck in industrial object perception. We briefly review DA and DR approaches, as well as their contribution towards narrowing the sim-to-real gap.

A. Domain Adaptation for Contextualized Synthetic Data

Contextualization is the alignment of synthetic scenes to the target deployment. Plausible approaches investigate the effect of calibrated geometry and materials [18], illumination [15], and image-space generative data diversification [19]. Such anchoring is associated with more relevant synthetic features, leading to reduced data requirements and smaller sim-to-real gaps [2].

Accurate CAD models, common in manufacturing, provide an initial geometrical reference [2]. However, geometric finetuning and manual texture matching usually require multiple modeling iterations and expert knowledge. Moreover,

in the absence of CAD models, 3D brownfield replication becomes more laborious and costly. In this context, novel GenAI methods such as TRELIS [11] and MeshyAI [12], as well as 3D reconstruction methods (e.g., 3D Gaussian Splatting [7]), have the potential to provide a practical substitute for target geometry modeling. However, research on their real-to-sim capabilities for 3D simulations and fully-synthetic industrial dataset creation is limited. Thus, this paper tackles this research gap by benchmarking multiple scan-based reconstruction pipelines and reporting their mAP outcomes, providing quantitative evidence amid scarce implementations and systematic evaluations.

Feature-space analyses using DINO embeddings [2] show that improved alignment between synthetic and target distributions correlates with higher detection accuracy. Physically grounded poses and contextual scene constraints implicitly enhance this alignment, as reflected by mAP and class-wise AP on real data. In contrast, pixel-space augmentations provide limited gains [19], motivating a focus on calibrated 3D context prior to constrained DR/GDR and rendering.

Our work builds on this techniques for DA. In addition, context-aware DR, i.e. GDR is applied to induce realistic variability while preserving task semantics.

B. Domain Randomization and the Simulation-to-Reality Gap

Industrial DR aims to mitigate the Simulation-to-Reality gap by expanding the synthetic training distribution through contained perturbations of illumination, materials, sensor noise, camera parameters, pose, and clutter, such that real images fall within the induced variability [20]. In industrial detection, this strategy has been supported by studies contrasting physics-based rendering against randomization [18], fully synthetic training pipelines with structured scene priors [21], and sim-to-real evaluations in robotics [13]. Yet published configurations are frequently tailored to a specific line, sensor, and part taxonomy, and broader evaluations indicate high sensitivity to design choices and limited portability [22]. Recent data-centric benchmarks with synthetic industrial data further suggest that performance depends strongly on how variability is instantiated and bounded rather than on detector choice alone [15]. This motivates pairing bounded, context aware randomization with GDR and DA, which explicitly aligns simulated and real feature distributions when residual appearance mismatch cannot be covered by randomization alone.

III. LOW-OVERHEAD 3D DOMAIN ADAPTATION

The first stage to create synthetic data with real-world relevant features is to acquire, create or generate 3D assets and corresponding textures that contain geometrical and color/texture information matching to some extent those of the real world. Previous approaches typically relied on CAD models and manual [15], [21], randomized [13], [14] or mixed [18] texture application. However, CAD models are not always available and manual modeling of synthetic assets with precise geometry and materials is both time-intensive

and demands specialized expertise. Thus, as shown in the DA stage of Fig. 1, we explore novel, low-overhead techniques for accurate 3D asset generation from physical objects. Fig. 2 compares four approaches for 2D-to-3D transformation with increasing levels of automation and decreasing human effort.

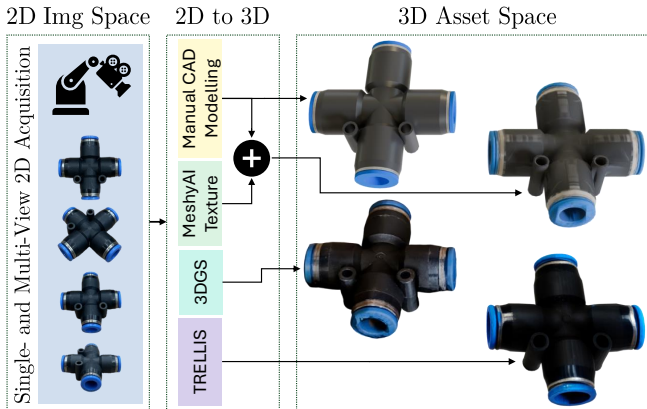


Fig. 2: 3D asset and texture generation as DA approaches.

Empirically evaluating the pipelines illustrated in Fig. 2 on all IRIS classes allows us to compare bidirectional sim-real transfer towards low-overhead domain-adapted synthetic data generation. In the following, we offer a brief description of the four pursued approaches:

a) *Manual Modeling*: high-quality CAD representations are modeled from physical functional shapes or retrieved, with written permission, from their intellectual property holders. Then, hand-crafted Physically Based Rendering (PBR) materials [23] are applied in Blender to visually represent the aspect of physical parts. This method provides ideal digital twins, but it is time-consuming, requires expert knowledge and misses part-production artifacts and imperfections.

b) *Manual CAD + MeshyAI*: accurate CAD geometry is kept, and PBR materials are generated automatically from a single real RGB image using MeshyAI [12]. Resulting textures are wrapped on the CAD objects. This method offers a good compromise between ideal geometry and realistic texture. Moreover, since only one image is required for texture generation, it constitutes a fast method that can be easily automated.

c) *3DGS*: multi-view images are collected from a physical part. Then a 3D Gaussian Splatting pipeline [7] implemented in the KIRI Engine [24] generates 3D mesh representations (geometry + textures). This method avoids manual texturing and produces meshes with a realistic appearance. However, introduced geometric artifacts require post-processing, comprising data cleaning and noise removal.

d) *TRELIS*: both mesh and texture are generated with the TRELIS model [11] directly from one or multiple input images. If CAD models are not available, this is the fastest tested method to generate semantically-correct 3D assets. However in our empirical experiments we observed that geometry and texture are dependent on image perspectives,

resulting in less consistency than the other approaches.

In addition to modeling of target objects, the impact of background realism is also evaluated using 3DGS. This approach offers an alternative to manual or randomized scene generation. This method aims at offering contextualized background information from the real test environment. In addition, it delves into the question of how much domain gap comes from object appearance versus scene context. A benchmark of the bidirectional sim-real capabilities of these methods is offered in subsection VI-D.

IV. SYNTHRENDER FRAMEWORK

The SynthRender framework is a programmatic generator of synthetic data with a sim-to-real transfer focus. As illustrated in the first stage of Fig. 3, it takes three main inputs: i) a configuration file defining the parameters listed in Table I, ii) 3D meshes or CAD models of the target objects for which annotations will be generated, and iii) contextual scene information, including textures, High Dynamic Range Image (HDR) files [25], and distractor objects. Each loaded model may appear multiple times per scene at randomized poses to increase data diversity and scene complexity.

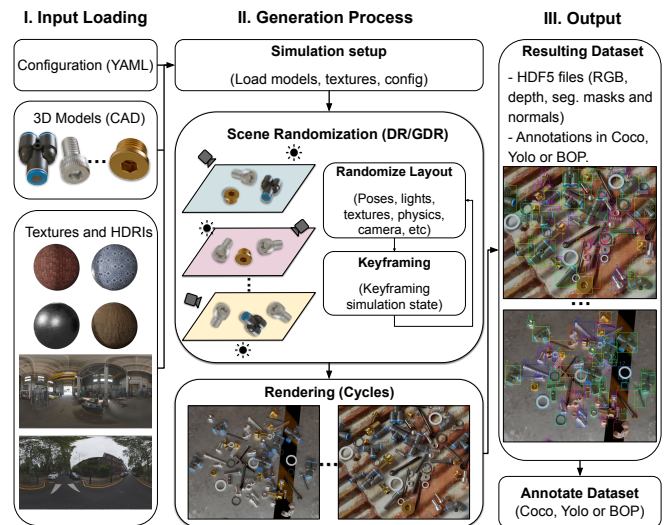


Fig. 3: Functional diagram of SynthRender, illustrating the input, generation, and output stages.

As depicted in the second stage of Fig. 3, SynthRender applies DR or GDR according to user-defined rules and ranges. Each frame has a unique, temporally discontinuous configuration of layout and simulation parameters. Both simulation and rendering are executed in Blender through the BlenderProc API, leveraging the Cycles path tracing engine [26].

For each randomized scene, metadata is computed during rendering and later used to generate the corresponding annotations, as shown in the third stage of Fig. 3. After rendering, RGB images and metadata are stored in HDF5 files. Each file contains RGB images, depth maps, normal maps, segmentation masks, and the parameter values used

for each frame. The following subsections describe the main components of the pipeline.

A. Load and process data

The framework loads a configuration file that defines all internal simulation parameters, including paths to CAD models, materials, and DR settings. Each CAD model undergoes preprocessing to ensure compatibility with the framework. Models are parented to a textureless cube-like proxy mesh used for faster collision-free placement. Optionally, all sub-parts of a model can be merged into a single mesh. Additional attributes, such as scale, texture, and category identifiers for annotation, are also assigned at this stage.

Fake models can be added to the scene. These are altered versions of existing assets and are used as distractors. They may consist of simple geometric primitives or deformed copies of real CAD models. Deformations modify the geometry while preserving the original texture, ensuring visual similarity without semantic equivalence.

Finally, auxiliary simulation elements are loaded, including a default digital twin scene, area lights arranged in a three-point studio configuration, and HDRI environment maps. If enabled, rigid body physics are assigned to all models. Target and fake models use active rigid bodies, while distractors use passive rigid bodies.

B. Set-up random scene

A total of n scenes are generated according to the configuration parameters shown in Table I. Randomization affects model visibility, collision-free placement, lighting intensity, and color. To improve rendering efficiency, each randomized scene state is mapped to a unique keyframe on the animation timeline.

As summarized in Table I, the following parameters are randomized during simulation:

- **Environmental background:** HDRI images are randomly selected as world backgrounds. Since HDRIs cannot be keyframed, scenes are rendered in batches sharing the same HDRI.
- **World lighting:** The HDRI light intensity is randomly sampled within a user-defined range.
- **Plane sampling:** Material variation is simulated by toggling the visibility of plane meshes associated with different materials.
- **Anchor pose:** The anchor position and rotation are randomly sampled from a spherical volume defined in the configuration file.
- **Camera:** The camera always points toward the anchor. Its position is sampled from a spherical volume around it, and depth of field is randomized via the f-stop parameter.
- **Area lights:** A three-point lighting setup is used. Light positions and directions follow the anchor pose, while color and intensity are randomized.
- **Target models:** Selected target models are placed within a cubic volume centered at the anchor. Placement is validated to avoid collisions and ensure visibility.

TABLE I: SynthRender Available Parameters for DR and GDR

Parameter	Range	Unit	Description
General Settings			
Output format	{seg, rgb, norm}	–	Output data channels
Physics	{0, 1}	Bool	Physics simulation
Background light	$s \geq 0$	–	Env. light intensity
Anchor Spawn			
Center	$c \in \mathbb{R}^3$	m	Anchor center
Radius	$r \geq 0$	m	Anchor radius
Elevation	$\epsilon \in [-90, 90]$	°	Elevation angle
Cam & Lighting			
Camera elevation	$\epsilon \in [-90, 90]$	°	Cam-to-anchor angle
Camera distance	$r \geq 0$	m	Distance to anchor
Light distance	$r \geq 0$	m	Distance to anchor
Light intensity	$E \geq 0$	W/m ²	Irradiance
Light exponential	$e \geq 0$	–	Falloff factor
Light color rand.	{0, 1}	Bool	Random RGB color
Object Spawn			
Target count	$n \in [\min, \max]$	–	Number of targets
Distractor count	$n \in [\min, \max]$	–	Number of distractors
Fake count	$n \in [\min, \max]$	–	Fake model count
Position	$p \in [\min, \max]^3$	m	Offset from anchor
Orientation	$\theta \in [-180, 180]^3$	°	3D Euler orientation
Object Config			
Join children	{0, 1}	Bool	Merge to single mesh
Scale	–	–	Object scale factor
Copies	–	–	Copies per object

- **Distractor models:** Real and fake distractors are sampled independently and placed within a user-defined volume. Placement is validated to avoid collisions and camera exclusion.

C. Render randomized scenes

Once all scenes have been generated, only the relevant frames are rendered, as shown in the output stage of Fig. 3. Rendering is restricted to an interval $[f_s, f_e]$, with $0 \leq f_s \leq f_e \leq n - 1$, avoiding rendering outside the region of interest. Furthermore, the pipeline renders multiple outputs simultaneously, including RGB images, semantic and instance segmentation masks, depth maps, normal maps, and simulation metadata containing poses, lighting parameters, and camera settings.

V. THE INDUSTRIAL REAL-SIM IMAGERY SET

IRIS is an industrial dataset containing 32 object classes, corresponding to mechanical and pneumatic components commonly found in industrial automation setups. All objects are shown in Fig. 4. IRIS follows a structured naming scheme to ensure clarity and traceability across all object classes. Each object identifier encodes both the component provenance (prefix) and, when applicable, its relative scale (suffix). Table II shows the object classes along their system-level categorization and the source of every CAD model.

IRIS is designed to evaluate object detection under realistic sensing conditions and to study sim-to-real transfer using high-quality synthetic assets. The objects in IRIS feature a unique set of characteristics:



Fig. 4: IRIS objects. Synthetic renders of the 32 industrial CAD models used in this study.

TABLE II: Object classes, source and system-level family.

ID	Class Name	Source	Family
1	C.O.Ring_L	Custom-Modeled	Mechanical
2	C.O.Ring_M	Custom-Modeled	Mechanical
3	C.O.Ring_S	Custom-Modeled	Mechanical
4	C.Plastic_Washer_L	Custom-Modeled	Mechanical
5	C.Plastic_Washer_S	Custom-Modeled	Mechanical
6	C.Steel_Ball_L	Custom-Modeled	Mechanical
7	C.Steel_Ball_S	Custom-Modeled	Mechanical
8	C.Washer_M5	Custom-Modeled	Mechanical
9	C.Washer_M6	Custom-Modeled	Mechanical
10	F.Roll-in_Nut_M5	FATH GmbH	Mechanical
11	FestoI	Festo SE & Co. KG	Pneumatic
12	FestoT	Festo SE & Co. KG	Pneumatic
13	FestoTorch	Festo SE & Co. KG	Pneumatic
14	FestoV	Festo SE & Co. KG	Pneumatic
15	FestoX	Festo SE & Co. KG	Pneumatic
16	FestoY	Festo SE & Co. KG	Pneumatic
17	GF_Collar_L	GlobalFastener Inc.	Mechanical
18	GF_Collar_S	GlobalFastener Inc.	Mechanical
19	GF_Slotted_Pin_L	GlobalFastener Inc.	Mechanical
20	GF_Slotted_Pin_S	GlobalFastener Inc.	Mechanical
21	GF_Split_Pin_L	GlobalFastener Inc.	Mechanical
22	GF_Split_Pin_S	GlobalFastener Inc.	Mechanical
23	GF_Cone_Screw_M8	GlobalFastener Inc.	Mechanical
24	GF_Hexagon_Nut	GlobalFastener Inc.	Mechanical
25	GF_Knurled_Screw_M8	GlobalFastener Inc.	Mechanical
26	GF_Plain_Screw_M8	GlobalFastener Inc.	Mechanical
27	GF_Screw_M5	GlobalFastener Inc.	Mechanical
28	MM_Silencer_L	McMaster-Carr Supply Co.	Pneumatic
29	MM_Silencer_S	McMaster-Carr Supply Co.	Pneumatic
30	MM_Spring	McMaster-Carr Supply Co.	Mechanical
31	MM_Wing	McMaster-Carr Supply Co.	Mechanical
32	MM_Wood_Screw	McMaster-Carr Supply Co.	Mechanical

- **Semi-Uncontrolled Conditions:** Multiple materials, geometries, sizes and textures are represented. In addition, environmental variations such as direct sunlight, camera-object poses, and changing backgrounds are introduced.
- **Extensible and Realism:** The selected 32 objects are industrial parts (e.g., pneumatic, fasteners, seals) and thus widely accessible for anyone interested in contributing with additional test data in new environments and with their own imaging systems.
- **Challenging Class Selection:** Objects share inter-class similarities in materials or geometries, increasing classification difficulty. Additionally, multiple instances per

class are present in the test set to introduce intra-class deviations (e.g., scratches, rust). These two features, in combination with varying environmental conditions represent a particularly challenging dataset for sim-real algorithms to effectively differentiate between object classes.

The 3D representations of the 32 mechanically-relevant components are collected from five sources, as per Table II. All objects include ideal 3D geometry from CAD models and 2D-to-3D reconstructed models from all methods investigated in this work (i.e., 3DGS, TRELIS, and MeshyAI-textured CADs). This unique systematic collection of perfect and reconstructed geometries with manual and reconstructed textures and annotated real RGB-D imagery counterparts enable systematic evaluation of novel bidirectional sim-real approaches. Moreover, a series of 2D scans used as input for the generative models are included in the dataset. This facilitates expanding the benchmark of GenAI models without physically sourcing the parts.

The real dataset contains 508 RGB-D images and about 20,000 annotations. Real images are captured at 1024×1024 resolution with a Zivid 2 Plus MR60 RGB-D sensor. The test scenes cover single- and multi-object detection across four acquisition domains, as shown in Table III. Real images include COCO/YOLO bounding boxes, while synthetic data provides pixel-perfect depth, instance masks, and 6D poses.

TABLE III: Number of real test images scene distribution

Controlled	Sunlight	Backgrounds	Robot	Total
101	67	100	240	508

VI. EXPERIMENTAL RESULTS AND ANALYSIS

This section presents sim-to-real experiments on three datasets: robotics [13], automotive [15], and IRIS. We evaluate the effect of the detection model and perform multiple ablation studies to identify the decisive factors that influence the sim-to-real gap. Finally, we compare our results with the state-of-the-art. All training experiments are run three times, and the reported values are averaged. In line with our data-centric approach, hyperparameter tuning and architecture search are outside the scope; training is conducted using the standard hyperparameters from the original model repositories.

A. SynthRender Across Detector Architectures

In these experiments, we evaluate the sim-to-real capabilities of SynthRender to generalize across three state-of-the-art object detection models: Yolov8 [5], Yolov11, and DEIM [6]. In this context, we generated a baseline synthetic dataset of 4k images with 1024×1024 pixel resolution and evaluated it on IRIS. Here, we use CAD models as geometric references and assign textures manually to the target objects. As the goal of this experiment is to validate the sim-to-real capabilities of SynthRender across multiple detector architectures using identical synthetic training data, neither RGB light randomization, exponential light sampling,

nor physics simulation from Table I are applied. These parameters are evaluated in ablation studies in subsequent sections. A dependency between model size (n, s, m, l, x) and mAP@50 is observed in Fig. 5. However, a comparable final mAP@50 is obtained for all model families, indicating architecture-agnostic sim-to-real transfer.

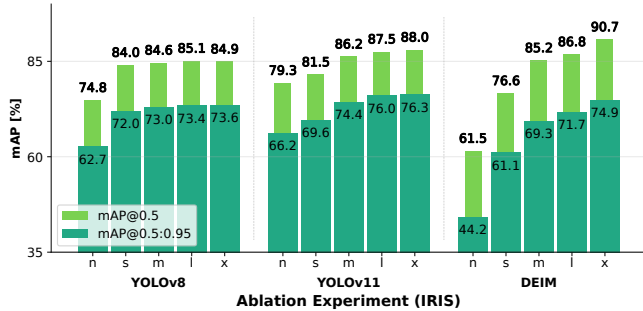


Fig. 5: SynthRender on three SOTA object detection models.

B. Ablation Studies: SynthRender Randomization Parameters

In a series of ablation studies, we evaluate which randomization, using SynthRender, and low-overhead adaptation, with CAD reconstruction, strategies help reduce the sim-to-real gap. Fig. 6 shows a positive development of mAP values across the robotics [13] and automotive [15] datasets if RGB light color randomization is enabled. A second test is conducted in which we allow exponential sampling of light intensities within the allowed randomization range. This translates into a synthetic dataset with brighter pixel distributions. Activating both light parameters improved mAP performance on the automotive dataset but did not improve performance on the robotics dataset compared to using only RGB light randomization.

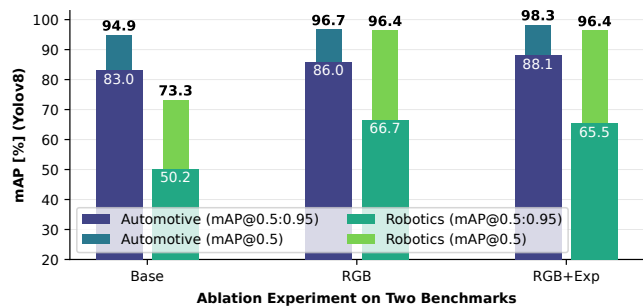


Fig. 6: Ablation experiments on the automotive [15] and robotics [13] benchmarks.

Fig. 7 builds on the results of Fig. 6 and expands the ablation parameters on the IRIS dataset. For instance, beyond RGB light randomization and exponential light sampling, physics simulation is enabled, showing on its own a larger positive effect on mAP values than the former two variables together. Moreover, if RGB randomization, exponential light sampling and physics are combined, mAP results improve

further. Similarly, if camera intrinsics are randomized within plausible ranges, a positive trend is also observed. Lastly, if instead of manually-selected textures for the target object, randomized PBR materials are allowed, a lower sim-to-real gap is exhibited, achieving the best results on the IRIS dataset with an mAP@50 = 95.3 and mAP@50-95 = 83.9. To ensure reproducibility, the synthetic images generated with SynthRender for the two best-performing results in Fig. 7 are publicly available as part of the IRIS dataset.

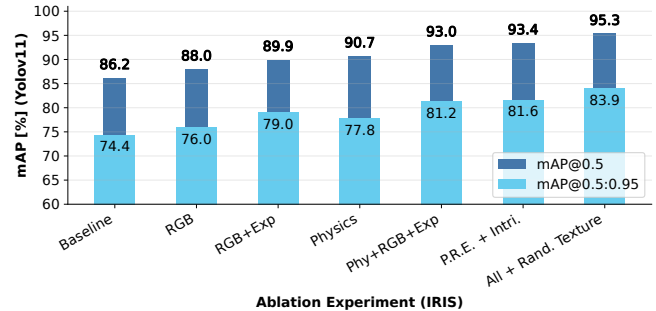


Fig. 7: Ablation study on IRIS with SynthRender parameters.

Moreover, Fig. 8 compares the distributions of mAP@50, precision, and recall for the top-performing datasets from Fig. 7. The lowest-performing IRIS classes are labeled in each metric. Precision distributions exhibit similar patterns across both datasets; however, mAP@50 and recall curves show more outliers and lower mean values in the manual dataset, particularly for the C_Steel_Ball_X classes. These results suggest that randomized textures are advantageous for highly reflective surfaces, as the detection model is forced to rely on geometric cues, which remain more consistent across synthetic and real environments.

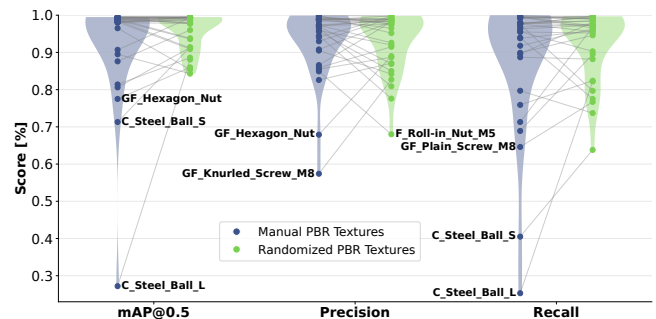


Fig. 8: Per-class performance comparison of IRIS objects after training with manual and randomized textures.

Figure 9 compares the effect of progressively reducing the number of synthetic training images for our two best-performing synthetic datasets from Fig. 7. For both datasets, mAP@50 and mAP@50-95 increase in proportion to the amount of images in the train set. However, performance gains become smaller as more data samples are allowed. Major performance gains are attained at low thousands image regime, with both datasets retaining competitive accuracy in

small train sets. This demonstrates that high-fidelity synthetic assets can be effective even in low-data regimes.

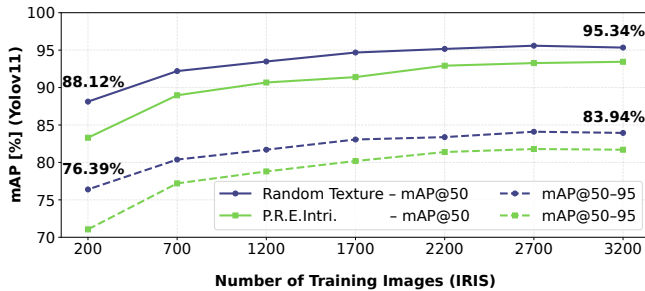


Fig. 9: Ablation on IRIS training set size (200–3200 images) using our two best-performing synthetic configurations.

C. Few-Shot Finetuning on Fully-Synthetic Models

Table IV summarizes the effect of adding a small number of real samples to synthetic training data across our two best synthetic datasets. Both datasets show consistent improvement with additional real images, demonstrating the value of few-shot adaptation. For the Random Texture dataset, performance improves from 95.36 mAP@50 (0-shot) to 98.80 mAP@50 (10-shot), with similar gains in mAP@50-95. The Physics-Based Rendering with Intrinsic (P.R.E.Intri.) dataset shows even more pronounced improvement, gaining 5.28% mAP@50-95 with 10 real samples (81.66% to 90.12%).

These results confirm that even a single real image provides measurable improvement over pure synthetic training, and 5 real images are sufficient to bridge most of the sim-to-real gap, achieving over 98% mAP@50 on both datasets.

TABLE IV: Few-shot results on IRIS with 4000 synthetic images. Zero-shot uses only synthetic data; few-shot setups add 1–10 real samples to the training dataset.

Dataset	mAP	Number of real images				
		0	1	3	5	10
Random Texture	@50	95.36	97.06	97.89	98.47	98.80
	@50-95	83.94	85.86	88.06	89.26	89.72
P.R.E.Intri.	@50	93.42	95.85	97.54	98.25	98.70
	@50-95	81.66	84.87	87.54	89.19	90.12

D. Low-Overhead 3D Domain Adaptation Results

Table V compares the results of the methods described in Section III. As expected, manually modeled CAD geometries, whether with manual or randomized textures, provide the strongest performance, but 3DGS reconstruction remains close, with only about a 2 mAP-point drop relative to the fully manual asset version. The lower-overhead, GenAI-based MeshyAI and TRELIS perform slightly lower, yet remain above 86% mAP@50. These results confirm that automated 2D-to-3D asset creation constitutes a valid alternative to manual modeling when CAD models are unavailable.

Furthermore, replacing randomized backgrounds with a more realistic scene setup using 3DGS scans of the real environment yields nearly identical performance. This aligns with

previous research suggesting that background adaptation is less critical for the detection model to transfer effectively to real-world scenarios [2] and locates 3DGS as an alternative to CAD-based scene creation.

TABLE V: Comparison of real-to-sim DA and randomization strategies.

Background	Target Objects		mAP@	
	Geometry	Texture	50	50-95
Randomized	Manual CAD	Randomized	95.34	83.94
	Manual CAD	Manual PBR	93.40	81.60
	3DGS Reconstr.	3DGS Reconstr.	91.21	80.04
	Manual CAD	MeshyAI GenAI	86.38	75.80
Reconstructed Scene (3DGS)	TRELIS GenAI	TRELIS GenAI	86.36	75.64
	Manual CAD	Manual PBR	93.26	81.36

E. Benchmarking Against the State-of-the-Art

We compare our approach against state-of-the-art methods across three benchmarks under matched experimental budgets. Table VI shows that our best-performing configuration with randomized PBR materials applied to CAD models outperforms prior results [14] on the robotics dataset [13] under matched training conditions, i.e. 4k images, 720 × 720 resolution, YOLOv8m detector. Further gains are possible by increasing the image resolution to 1024 × 1024.

TABLE VI: State-of-the-art comparison on fully-synthetic training of robotics [13], automotive [15] and proposed IRIS benchmarks.

Dataset	Method	mAP@		Test Conditions			
		50	50-95	Model	# Img	Res.	Texture
Robotics	Horváth [13]	83.2	–	Yolov4	4k	Variable	Rand. PBR
	Horváth [13]	84.5	–	Yolov4	8k	Variable	Rand. PBR
	Zhu [14]	88.4	–	Yolov4	4k	720 ²	Rand. PBR
	Zhu [14]	90.4	–	Yolov4	8k	720 ²	Rand. PBR
	Zhu [14]	96.1	–	Yolov8	4k	720 ²	Rand. PBR
	Zhu [14]	96.4	–	Yolov8	8k	720 ²	Rand. PBR
	Ours	99.1	70.4	Yolov8	4k	720 ²	Rand. PBR
	Ours	99.3	70.5	Yolov8	4k	1024 ²	Rand. PBR
Auto.	Araya [15]	–	75.0	Yolov8	900	512 ²	Manual
	Araya [2]	91.3	78.4	Yolov8	900	512 ²	Manual
	Ours	97.4	85.2	Yolov8	900	512 ²	Manual
	Ours	98.3	88.1	Yolov8	4k	512 ²	Manual
IRIS	SynMfg [14]	77.2	59.6	Yolov11	4k	1024 ²	Rand. PBR
	Ours	95.3	83.9	Yolov11	4k	1024 ²	Rand. PBR

Consistent improvements are also observed on the automotive benchmark [15] under identical test condition. Here, manually assigned textures are used instead of randomized PBR materials to match previously reported settings. Additionally, we evaluate the SynMfg [14] synthetic data generation pipeline on IRIS. Its standard configuration yields lower performance than SynthRender, as illustrated in Fig. 7. We note, however, that improved results may be attainable with more thorough parameter exploration and additional optimization of the SynMfg pipeline.

VII. CONCLUSIONS AND FUTURE WORK

We introduce SynthRender, a synthetic data generator, and IRIS, a dataset for bidirectional sim–real analysis in industrial settings. Across multiple benchmarks, we show that sim-to-real performance depends primarily on how synthetic variability is constructed and constrained, rather than on the choice of detection architecture.

Ablation studies reveal that bounded DR, combining physically plausible scene formation with diverse lighting spectra, nonlinear light intensity sampling, and randomized PBR materials, consistently outperforms baseline rendering. For highly-reflective objects, such as steel components, texture randomization encourages detectors to rely on transferable geometric cues, improving robustness. Accuracy scales with synthetic dataset size but saturates in the low-thousands-image regime, demonstrating strong data efficiency even under semi-uncontrolled IRIS conditions.

Few-shot fine-tuning further reduces the remaining sim-to-real gap. Adding only one to five real images yields most of the achievable improvement and reaches near-perfect mAP@50 in the best synthetic configurations. Among real-to-sim asset strategies, manually curated CAD models perform best, while 3D Gaussian Splatting achieves comparable results. Replacing randomized backgrounds with realistic scans has no measurable impact, indicating that 3DGS is a practical alternative when CAD assets are unavailable.

Finally, using SynthRender and our proposed data generation guidelines, we achieve state-of-the-art performance on two established industrial benchmarks under identical evaluation protocols. These results support a bidirectional sim-real workflow, where real observations refine assets and priors, and simulation provides controlled variability with minimal real supervision as the final calibrator.

As future work, we plan to exploit high-fidelity RGB-D data in IRIS and SynthRender’s rendering capabilities to further improve robustness and data efficiency in sim-to-real RGB-D perception. Extending the test set and performing a comprehensive performance analysis across multiple semi-uncontrolled IRIS scenarios could provide deeper insights into generalization and robustness in real-world conditions.

REFERENCES

- [1] F. Töper, J. M. Araya-Martinez, A. S. Reig, T. Tom, S. Sardari, and P. Ohlhausen, “Leveraging synthetic training data for object detection to enhance autonomous depalletizing systems,” in *European Robotics Forum*. Springer, 2025, pp. 229–235.
- [2] J. M. Araya-Martinez, T. Tom, S. Sardari, A. Sanchis Reig, G. Mohan, A. Shukla, F. Töper, J. Lambrecht, and J. Krüger, “Domain adaptation using vision transformers and xai for fully synthetic industrial training,” *Procedia CIRP*, vol. 135, 2025, 35th CIRP Design Conference.
- [3] B. Wen, W. Yang, J. Kautz, and S. Birchfield, “Foundationpose: Unified 6d pose estimation and tracking of novel objects,” in *Proceedings of the IEEE/CVF Conference on Computer Vision and Pattern Recognition*, 2024, pp. 17 868–17 879.
- [4] A. Kirillov, E. Minton, N. Ravi, H. Mao, C. Rolland, L. Gustafson, T. Xiao, S. Whitehead, A. C. Berg, W.-Y. Lo, P. Dollár, and R. Girshick, “Segment anything,” in *Proceedings of the IEEE/CVF International Conference on Computer Vision (ICCV)*, October 2023, pp. 4015–4026.
- [5] M. Hussain, “Yolo-v1 to yolo-v8, the rise of yolo and its complementary nature toward digital manufacturing and industrial defect detection,” *Machines and Tooling*, vol. 11, p. 677, 2023.
- [6] S. Huang, Z. Lu, X. Cun, Y. Yu, X. Zhou, and X. Shen, “Deim: Detr with improved matching for fast convergence,” in *Proceedings of the IEEE/CVF Conference on Computer Vision and Pattern Recognition (CVPR)*, June 2025, pp. 15 162–15 171.
- [7] R. Tobiasz, G. Wilczyński, M. Mazur, S. Tadeja, and P. Spurek, “Mesh-splats: Mesh-based rendering with gaussian splatting initialization,” *arXiv preprint arXiv:2502.07754*, 2025.
- [8] M. Denninger, D. Winkelbauer, M. Sundermeyer, W. Boerdijk, M. Knauer, K. H. Strobl, M. Humt, and R. Triebel, “Blenderproc2: A procedural pipeline for photorealistic rendering,” *Journal of Open Source Software*, vol. 8, no. 82, p. 4901, 2023. [Online]. Available: <https://doi.org/10.21105/joss.04901>
- [9] E. Coumans, “Bullet physics library,” <https://github.com/bulletphysics/bullet3>, accessed: 2025-02-01.
- [10] T. B. Foundation, “Blender 4.0,” 2023, <https://projects.blender.org/blender/blender.git> [Accessed: (12.06.2025)].
- [11] J. Xiang, Z. Lv, S. Xu, Y. Deng, R. Wang, B. Zhang, D. Chen, X. Tong, and J. Yang, “Structured 3d latents for scalable and versatile 3d generation,” *arXiv preprint arXiv:2412.01506*, 2024.
- [12] MeshyAI Team, “Meshy ai - the #1 ai 3d model generator,” <https://www.meshy.ai/discover>, 2025, accessed: 2025-11-18.
- [13] D. Horváth, G. Erdős, Z. Istenes, T. Horváth, and S. Földi, “Object detection using sim2real domain randomization for robotic applications,” *IEEE Transactions on Robotics*, vol. 39, no. 2, pp. 1225–1243, 2022.
- [14] X. Zhu, J. Henningsson, D. Li, P. Mårtensson, L. Hanson, M. Björkman, and A. Maki, “Domain randomization for object detection in manufacturing applications using synthetic data: A comprehensive study,” in *2025 IEEE International Conference on Robotics and Automation (ICRA)*, 2025.
- [15] J. M. Araya-Martinez, S. Sardari, M. Lambert, J. A. Zak, F. Töper, J. Krüger, and J. Lambrecht, “A data-centric evaluation of leading multi-class object detection algorithms using synthetic industrial data,” in *Advances in Automotive Production Technology – Digital Product Development and Manufacturing*, D. Holder, F. Wulle, and J. Lind, Eds. Cham: Springer Nature Switzerland, 2025, pp. 283–302.
- [16] M. Everingham, L. Van Gool, C. K. Williams, J. Winn, and A. Zisserman, “The pascal visual object classes (voc) challenge,” *International journal of computer vision*, vol. 88, pp. 303–338, 2010.
- [17] T.-Y. Lin, M. Maire, S. Belongie, J. Hays, P. Perona, D. Ramanan, P. Dollár, and C. L. Zitnick, “Microsoft coco: Common objects in context,” in *Computer Vision—ECCV 2014: 13th European Conference, Zurich, Switzerland, September 6–12, 2014, Proceedings, Part V 13*. Springer, 2014, pp. 740–755.
- [18] L. Eversverg and J. Lambrecht, “Generating images with physics-based rendering for an industrial object detection task: Realism versus domain randomization,” *Sensors*, vol. 21, no. 23, p. 7901, 2021.
- [19] J. M. Araya-Martinez, A. Sanchis Reig, G. Mohan, S. Sardari, J. Lambrecht, and J. Krüger, “Synthetic industrial object detection: Genai vs. feature-based methods,” *Procedia CIRP*, 2025, 19th CIRP Conference on Intelligent Computation in Manufacturing Engineering, in press.
- [20] J. Tobin, R. Fong, A. Ray, J. Schneider, W. Zaremba, and P. Abbeel, “Domain randomization for transferring deep neural networks from simulation to the real world,” in *2017 IEEE/RSJ international conference on intelligent robots and systems (IROS)*. IEEE, 2017, pp. 23–30.
- [21] C. Mayershofer, T. Ge, and J. Fottner, “Towards fully-synthetic training for industrial applications,” in *LISS 2020*. Springer Singapore, 2021, pp. 765–782.
- [22] X. Zhu, T. Bilal, P. Mårtensson, L. Hanson, M. Björkman, and A. Maki, “Towards sim-to-real industrial parts classification with synthetic dataset,” in *2023 IEEE/CVF Conference on Computer Vision and Pattern Recognition Workshops (CVPRW)*, 2023, pp. 4454–4463.
- [23] M. Pharr, W. Jakob, and G. Humphreys, *Physically Based Rendering: From Theory to Implementation*, 3rd ed. San Francisco, CA: Morgan Kaufmann, 2016.
- [24] Kiri Engine Team, “Kiri engine: 3d scanner app for iphone, android, and web,” <https://www.kiriengine.app/>, 2025, accessed: 2025-10-25.
- [25] P. E. Debevec and J. Malik, “Recovering high dynamic range radiance maps from photographs,” in *Proceedings of SIGGRAPH 1997*, 1997, pp. 369–378.
- [26] B. Foundation, “The cycles render engine,” 2023, <https://projects.blender.org/blender/cycles.git> [Accessed: (12.06.2025)].